AD-A212 522

DOCUMENTATION PAGE

Form Approved -OMB No. 0704-0188

1b. RESTRICTIVE MARKINGS

2a. SECURITY CLASSIFICATION AUTHORITY

2b. DECLASSIFICATION / DOWNGRADING SCHEDULE

3. DISTRIBUTION / AVAILABILITY OF REPORT
Approved for public release; distribution is unlimited.

4. PERFORMING ORGANIZATION REPORT NUMBER(S)

5. MONITORING ORGANIZATION REPORT NUMBER(S)
AFATL-TP-89-17

6a. NAME OF PERFORMING ORGANIZATION	6b. OFFICE SYMBOL (If applicable)	7a. NAME OF MONITORING ORGANIZATION
Aerodynamics Branch Aeromechanics Division	AFATL/FXA	Aerodynamics Branch Aeromechanics Division

6c. ADDRESS (City, State, and ZIP Code)	7b. ADDRESS (City, State, and ZIP Code)
Air Force Armament Laboratory Eglin AFB, FL 32542-5434	Air Force Armament Laboratory Eglin AFB, FL 32542-5434

8a. NAME OF FUNDING / SPONSORING ORGANIZATION	8b. OFFICE SYMBOL (If applicable)	9. PROCUREMENT INSTRUMENT IDENTIFICATION NUMBER
Aeromechanics Division	AFATL/FXA	

8c. ADDRESS (City, State, and ZIP Code)	10. SOURCE OF FUNDING NUMBERS			
	PROGRAM ELEMENT NO.	PROJECT NO.	TASK NO.	WORK UNIT ACCESSION NO.
Air Force Armament Laboratory Eglin AFB, FL 32542-5434	62602F	2567	03	12

11. TITLE (Include Security Classification)

Aerodynamic Test and Analysis of a Slender Generic Missile Configuration

12. PERSONAL AUTHOR(S)
Roger S. Gates, G.L. Winchenbach, John R. Cipolla, and Mark A. Fische

13a. TYPE OF REPORT	13b. TIME COVERED	14. DATE OF REPORT (Year, Month, Day)	15. PAGE COUNT
Interim	FROM Nov 87 TO Aug 89	September 1989	10

16. SUPPLEMENTARY NOTATION

AIAA Atmospheric Flight Mechanics Symposium Boston, MA - August 1989

17. COSATI CODES			18. SUBJECT TERMS (Continue on reverse if necessary and identify by block number)
FIELD	GROUP	SUB-GROUP	
			Free Flight Aerodynamics, Computational Fluid Dynamics, Supersonic, Static-Dynamic Stability.

19. ABSTRACT (Continue on reverse if necessary and identify by block number)

This paper discusses the aerodynamic predictions, tests, and analyses of a slender fin stabilized missile configuration at Mach numbers from 1.0 to 5.0. Prediction techniques consisted of both empirical and analytical methods, including state-of-the-art computational fluid dynamic codes. Free flight tests were also conducted on subscale models to obtain an aerodynamic baseline to which the various predictions could be compared. This paper summarizes these results, attempts to identify the physics governing the flight trajectories, and proposes new ideas for further research in this technology area.

89 9 15 004

20. DISTRIBUTION / AVAILABILITY OF ABSTRACT	21. ABSTRACT SECURITY CLASSIFICATION
☐ UNCLASSIFIED/UNLIMITED ☒ SAME AS RPT. ☐ DTIC USERS	Unclassified

22a. NAME OF RESPONSIBLE INDIVIDUAL	22b. TELEPHONE (Include Area Code)	22c. OFFICE SYMBOL
Gerald L. Winchenbach	(904) 882-4085	AFATL/FXA

DD Form 1473, JUN 86 — Previous editions are obsolete. — SECURITY CLASSIFICATION OF THIS PAGE UNCLASSIFIED

AERODYNAMIC TEST AND ANALYSIS OF A SLENDER GENERIC MISSILE CONFIGURATION

Roger S. Gates*, Gerald L. Winchenbach**, John R. Cipolla+
Aerodynamics Branch
Aeromechanics Division
Air Force Armament Laboratory
Eglin AFB FL
and
Mark A. Fischer++
Advanced Systems Engineering Group
General Electric Company
Burlington VT

Abstract

This paper discusses the aerodynamic predictions, tests, and analyses of a slender fin stabilized missile configuration at Mach numbers from 1.0 to 5.0. Prediction techniques consisted of both empirical and analytical methods, including state-of-the-art computational fluid dynamic codes. Free flight tests were also conducted on subscale models to obtain an aerodynamic baseline to which the various predictions could be compared. This paper summarizes these results, attempts to identify the physics governing the flight trajectories, and proposes new ideas for further research in this technology area.

Nomenclature

A	=	reference area, $d^2/4$
C_{lp}	=	roll damping derivative
C_{m_α}	=	pitching moment derivative
C_{mq}	=	pitch damping derivative
C_{N_α}	=	normal force derivative
C_{Xo}	=	zero yaw axial force coefficient
d	=	projectile body diameter (reference length)
l	=	projectile length
M	=	Mach number
p	=	spin rate
R_l	=	Reynolds number based on length
v	=	velocity
X	=	projectile longitudinal axis
X_{cg}/l	=	center of gravity location
X_{cp}/l	=	center of pressure location
$\bar{\delta}^2$	=	effective angle of attack squared

*Capt, USAF, Aeroballistics Section, Member AIAA
**Chief, Aeroballistics Section, Associate Fellow, AIAA
+Aerospace Engineer, Computational Fluid Dynamics Section, Member AIAA
++Advanced Systems Analyst

Background

Fin stabilized missile configurations are known to exhibit decreasing static stability as a function of increasing Mach number. Figure 1 shows a typical static stability plot where the missile's restoring moment continuously decreases, eventually leading to static instability (i.e. the pitching moment slope becomes positive). Because of the obvious advantages associated with increasing the speed of missile configurations, the Air Force Armament Laboratory (AFATL) initiated an in-house program to investigate potential methods to extend future flight regimes. However, before this could be accomplished it was believed that a substantially more detailed understanding of the flow physics creating this situation must be obtained. Therefore, the first phase of this program was to predict, substantiate, and understand the static stability characteristics of a generic missile configuration. This paper summarizes the current research which attempts to fulfill those goals. A corollary to this research is to begin identifying key missile geometry parameters (i.e. fin shape/size) which will effectively increase the stability envelope.

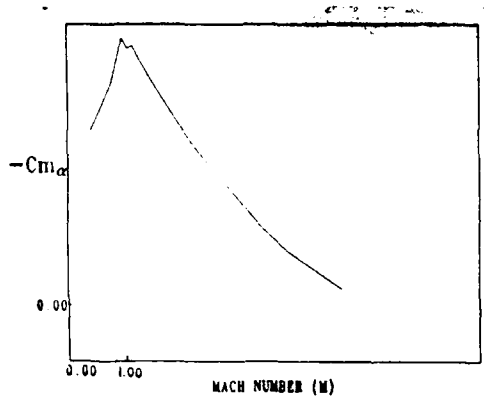

Fig. 1 Typical C_{m_α} versus Mach Number plot.

Test Configurations

In determining a configuration on which to conduct this research, it was decided to select a configuration which would most dramatically exhibit the static stability limitations previously described. Therefore, a generic, high fineness ratio, tail-controlled missile configuration was developed as the baseline model (Figure 2). The model consisted of an ogive nose, cylindrical body, with one four-fin group located near the extreme aft end of the projectile. Two separate fin configurations were fabricated for

the free flight tests, the difference being that the delta fin planform area of one configuration was exactly twice the area of the other (maintaining the fin aspect ratio). All fins were equally spaced at 90 degrees. The fin thickness (made of .015 inch shim stock) was small compared to the body diameter. The fabricated models were approximately 5 percent scale compared to current air-to-air missile configurations and had a fineness ratio (length to diameter) of 24 which is representative of today's air-to-air missiles. In addition to the two fin designs, models consisting of two separate center of gravity locations (approximately 43 and 52 percent length from the nose) were tested for each design. All models were constructed in-house and passed a quality control inspection prior to testing.

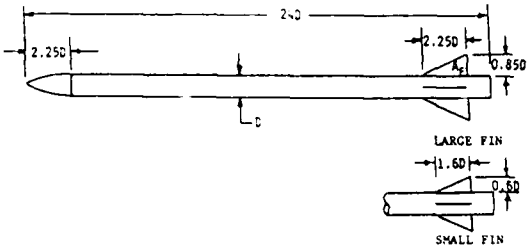

Fig. 2 Sketch of configurations.

The model/sabot packages were designed to be fired from a smoothbore 30mm barrel. A single stage powder gun was used to obtain flight data up to Mach 3.5 and a two-stage light gas gun[1] was utilized to achieve the flight data up to Mach 5.0. Figure 3 is a photograph of two model/sabot packages, showing both the large and small fin models. The sabot serves several important functions. It protects the model while inside the barrel during the launch cycle and forms a gas seal during the burning of the propellant so that consistent and maximum exit velocities are achieved. Upon exit from the barrel, the sabot pedals and pusher are stripped away and only the model is allowed to continue through the instrumented section of the test facility.

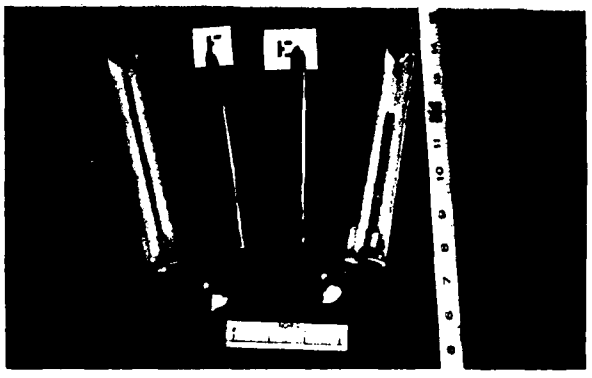

Fig. 3 Photograph of model/sabot packages.

Test Facilities

The free flight tests were conducted at the USAF Aeroballistic Research Facility (ARF), Eglin AFB, Florida. The ARF is an enclosed concrete structure used to examine the exterior ballistics of various munitions while in unrestrained flight.[2] The facility contains model measurement equipment, a launch room, a blast chamber (to strip away the sabot), an instrumentation control room, and the instrumented range. The range atmospheric conditions are closely monitored. The instrumented section of the ARF is 207 meters long. It has a 13.40 square meter cross-section for the first 69 meters and a 23.80 square meter cross-section for the remaining length. There are 131 locations available as instrumentation sites and each has a physical separation of 1.52 meters. Presently, 50 of those sites are used to house orthogonal shadowgraph stations. At each of these stations the maximum window (an imaginary circle in which a projectile in flight will cast a shadow on both orthogonal reflective screens) is 2.13 meters in diameter. The orthogonal photographs obtained of the model's shadow (called shadowgrams) are subsequently used to determine the spatial position and angular orientations of the projectile at each of the shadowgraph stations. The position, orientation, and time data are then used to reconstruct the experimental trajectory which is compared to the governing theoretical equations of motion in order to extract the aerodynamics of the test projectile. This is accomplished by using the Aeroballistic Research Facility Data Analysis System (ARFDAS).[3] ARFDAS is a user friendly data reduction code which enables the engineer to analyze, plot, and tabulate the aerodynamic results from each test flight. Figure 4 shows a typical flowfield photograph taken from a direct spark shadowgraph.

Fig. 4 Typical flowfield shadowgram of a small fin model in flight.

Prediction Techniques

Preceding the test flights, static stability predictions were made using both empirical and computational methods. The empirical predictions were made using the Projectile Design Analysis System (PRODAS)[4]. PRODAS is an interactive program which allows the engineer to create a projectile by specifying it's material and physical dimensions. It calculates the model physical properties and compares that design to similar configurations in an extensive data base. The program then interpolates the data base to provide estimated aerodynamic coefficients for the created configuration. The following data figures show these aerodynamic predictions for both the small and large delta fin configurations previously described.

The computational predictions were obtained by using two methods. First, an inviscid space marching Euler code was used to predict the stability characteristics for both configurations of interest between Mach 3.0 and 7.0. The Zonal Euler Solver (ZEUS)[5] code, is a finite volume, flow solver that uses shock fitting for the bow shock. It was selected because of its efficiency and robustness. The ZEUS code is especially suitable for computations in which the flow field is completely supersonic about the body and assumes that the fins are infinitely thin. The code applies a zonal strategy which divides the computational domain into zones which can be mapped separately. The zone edges are defined by the user to coincide with the body and bow shock surfaces.[6] The calculation of the flowfield is initiated near the nose tip of the body and marched aft in a planar fashion along the longitudinal axis of the body to its base. The initial flowfield was generated by a separate conical-flow starting solution. Three computational zones were established due to symmetry conditions. Two fins were defined in the half plane as presented in the sketch below.

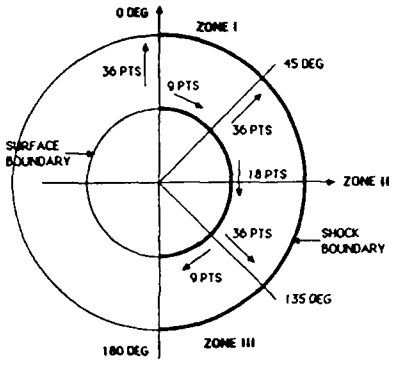

The two fins are located at the 45° and 135° positions, respectively, where 0° is defined in the sketch. A 9 X 36 grid was employed in zone 1, zone 2 employed a 18 X 36 grid and zone 3 used a 9 X 36 grid. The grids in the circumferential direction were equally spaced, while the 36 points used in the radial direction were clustered between the body surface and the bow shock wave. These cells were clustered so that grid points were concentrated close to the body. The step size in the marching direction, along the body axis, was automatically varied as a function of goemetry, flow condition and stability criteria.

The Eglin Arbitrary Geometry, Implicit Euler (EAGLE) Code, was used as another analytical method to predict static stability. This program is a multiblock grid generation and steady state flow solver system. It combines a boundary conforming surface generation scheme [7,8], a composite block structure grid generation scheme [9], and a multiblock implicit Euler flow solver algorithm.[10] The EAGLE code is used to obtain predictions for the flight regimes in which the flowfield is not necessarily entirely supersonic. The computational grid developed for the fin-stabilized missile discussed herein consisted of twelve (12) three-dimensional blocks for a total of 170,240 grid point locations. Three regions were defined in the grid generation process as existing between each of the four (4) fins at the rear of the missile. Each of the twelve blocks are defined by rotating the three regions between any two fins, a rotation of 90 degrees.

The grid points were clustered near the body surface using a hyperbolic tangent distribution starting with an initial spacing of .001 in. Two separate grid descriptions were generated, one for transonic flow (M = .8 to M = 1.2) and another for supersonic flow (M = 1.5 to M = 4.5). The dimensions of each grid field has been optimized for the characteristics of each flow regime. The grid for the transonic regime (M = 0.8 to 1.2) has been dimensioned to capture a Mach wave ($\mu = \sin^{-1} 1/M$) expected to propagate from a point source located at the nose-tip at Mach = 1.2 and intersecting a point located on the flow-exit plane. The Mach wave will intersect the flow-exit surface at the 60 percent point of the exit plane length, leaving space for the shock wave to be captured. The same reasoning was applied to the supersonic regime from Mach = 1.5 to Mach = 4.5 by selecting Mach = 2.5 as the baseline condition. Figure 5a is the cross-sectional view of the grid used for the supersonic series of Mach numbers (M = 1.5 to 4.5) and part b of Figure 5 is a cross-sectional view of the grid used for the transonic series of Mach numbers (M = .8 to 1.2). It was found that maximum grid density could be achieved by using the Mach wave to define the approximate location of the bow shock and adjusting the outer boundary to allow the shock wave to be captured during the time dependent solution.

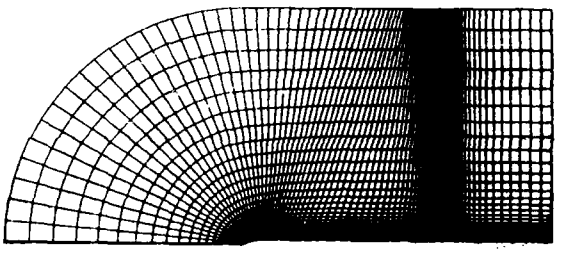

a. Supersonic Grid

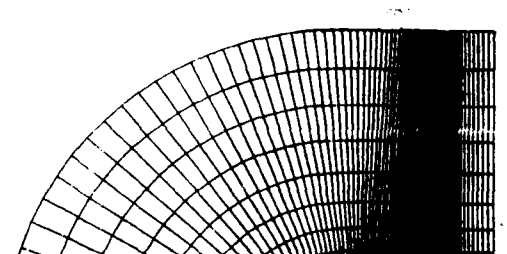

b. Transonic Grid

Fig. 5 EAGLE code grid.

The aerodynamic derivatives, C_{m_α} and C_{N_α}, were computed by differencing the normal force and moment coefficients at zero and 0.5 deg. angle of attack. The moment coefficient was obtained directly from the EAGLE code and the normal force coefficient was computed using the lift and drag coefficients as obtained from EAGLE, (ie, $C_N = C_L \cos\alpha + C_D \sin\alpha$). Since the fins were considered to be infinitely thin they were modeled by using the proper flow-field boundary conditions between the inter-connecting blocks in the EAGLE flow solver.

The results from both the ZEUS and EAGLE code predictions are plotted along with the PRODAS predictions in the following data figures. These predictions formed the baseline for the aerodynamic tests. The remainder of this paper will discuss the free flight test analysis, comparisons with the predictions, and the resulting conclusions.

Experimental/Computational Results

Tables 1 and 2 summarize the experimental results for the small and large fin model configurations and include both single and multiple fit reductions. The multiple fit is a technique where flights of the same configuration and at similar Mach number conditions are simultaneously analyzed. This provides a common set of aerodynamics that match each of the separately measured position-attitude-time profiles. This approach provides a broader range of angle of attack and roll orientation combinations than would be available from each trajectory considered separately. This increases the probability that the determined coefficients define the configuration's aerodynamics over a larger range of possible trajectories. There are blanks in the summary tables where that particular value was held fixed (for reasons that will be explained in subsequent discussions). This was done so that only experimentally determined coefficients would be shown in the Tables 1 and 2.

Pitching Moment Derivative

Figure 6 shows the experimentally determined pitching moment derivative for both the small and large fin configurations, respectively. Note the two distinct levels resulting from having two different center of gravity locations (as described earlier) in each of the plots. As expected, the forward center of gravity configurations exhibit greater stability which is exemplified by the more negative (parallel shift) derivative values. Based on this plot, one would expect the small fin (Xcg/l=.52) model to be statically unstable at approximately Mach = 2.2. As can be seen in Figure 7, which plots the angular motion versus travel for a model fired at this very condition, this is precisely what occurred. This particular flight was the only one purposely launched at such a condition because we did not want to risk damage to the ARF instrumentation systems.

The majority of the flights experienced relatively small angular motions, therefore the

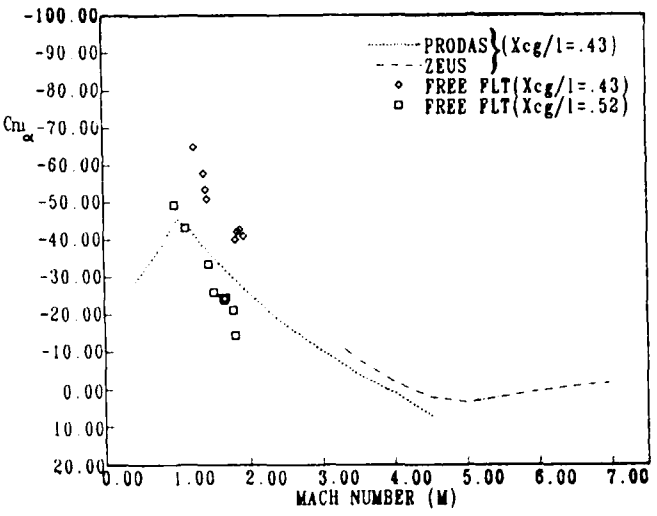

a. Small fin.

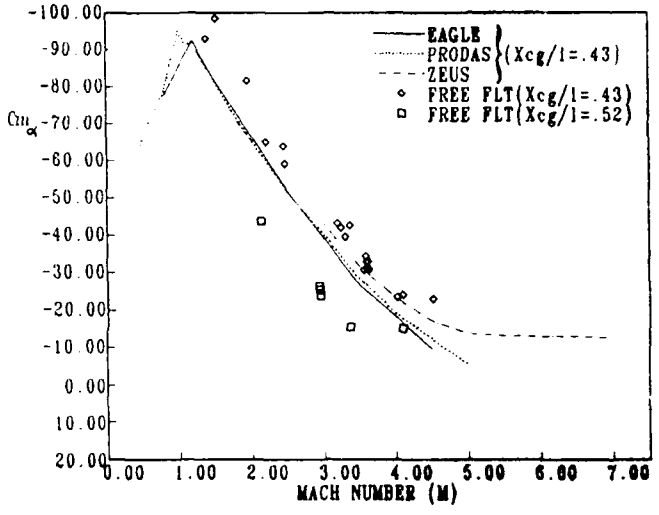

b. Large fin.

Fig. 6 Pitching moment derivatives.

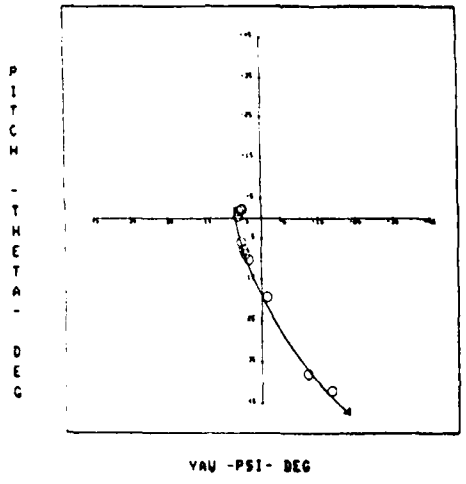

Fig. 7 Angular motion plot of statically unstable flight.

determination of non-linear pitching moment coefficients was not attempted for these. However, for flights that did have a significant angle of attack, an attempt to fit the non-linear terms was tried but these attempts were not successful. The small angular motions for many of these flights also made it more difficult to obtain accurate zero angle of attack coefficients, such as the first order pitching moment coefficient. Note that some Cm_{α} values in the tables have been deleted for this very reason. Additionally, notice that the Mach number dependent pitching moment term, $Cm_{\alpha M}$, can be easily obtained from the slopes of the curves in Figure 6. These values are approximately 40 and 30 for the small and large fin models respectively. It should be noted that the angular motion fit (to the flight trajectories) was not very dependent on having an accurate value for this coefficient.

Figure 6a displays the results for $C_{m_{\alpha}}$ as computed by ZEUS and PRODAS for the small fin model. The ZEUS and PRODAS results were computed for the X_{cg}/l = .43 location and not for the X_{cg}/l = .53. The PRODAS results are clearly underpredicting the $C_{m_{\alpha}}$ data for the free-flight measurements and the ZEUS code appears to predict these results better if the computations could be extended to the lower Mach numbers indicated by the test data. However, since ZEUS is a supersonic marching code and the available data is in the transonic range, M = .8 to M = 1.84, the ZEUS code would become numerically unstable because of the hyperbolic nature of the supersonic Euler equations. Therefore, direct computation in this range was not attempted using the ZEUS code. The apparant discrepancy between the free-flight data and the theoretical results indicate that fin size may have been a major factor in the difference. It is indicated that the boundary layer thickness at the end of the missile is thick enough to render the Prodas solution ineffective for the small fin model. Not much can be said about the Zeus results because the predictions do not extend far enough into the region covered by the free-flight data.

Figure 6b shows the results for $C_{m_{\alpha}}$ as predicted by EAGLE, ZEUS and PRODAS for the large fin configuration. The predictive techniques were executed for a Xcg/l reference location equal to 0.43. The EAGLE code and the PRODAS results are reasonably close over the entire range from M = .8 to M = 4.5 as displayed on the plot. It is significant that such good correlation with the free-flight data can be attained over a range of Mach numbers that extends from M = .8 to M = 4.5. Free Flight data is under-predicted to a small degree by all of the methods, but the trend in the data is captured by all of the CFD techniques. It is interesting to note that the ZEUS code seems to predict $C_{m_{\alpha}}$ better than either of the other two methods at the higher Mach numbers. The ZEUS data however, converges to EAGLE and PRODAS results as the Mach number is reduced below M = 3.

Normal Force Derivative

Because the force coefficient effects are more difficult to extract than moment derivatives from flights with little angular motion, the normal force coefficient was understandably harder to obtain from these flights. However, this was not unexpected, and was the reason that the two different center of gravity model configurations were fabricated. Figure 8 shows the determined normal force coefficient derivative using the multiple fit method previously discussed plotted versus Mach number for the small and large fin configurations. Also, shown in this figure, are empirically determined values obtained using the technique shown in Figure 9. This figure plots the experimentally determined pitching moment versus Xcg/l for Mach number = 1.2 (small fin model).

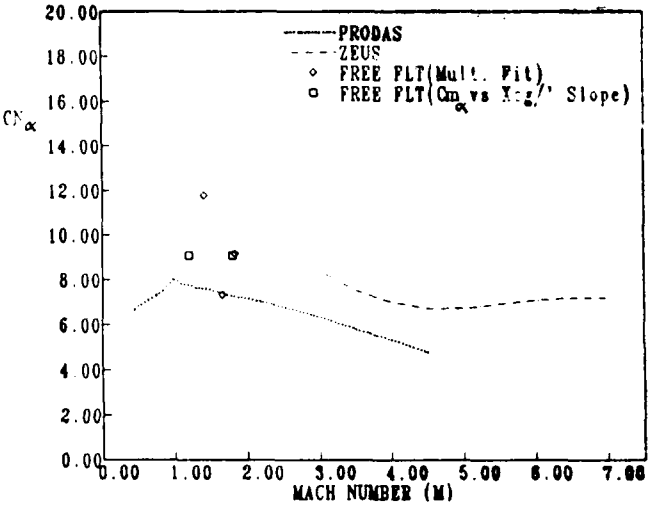

a. Small fin.

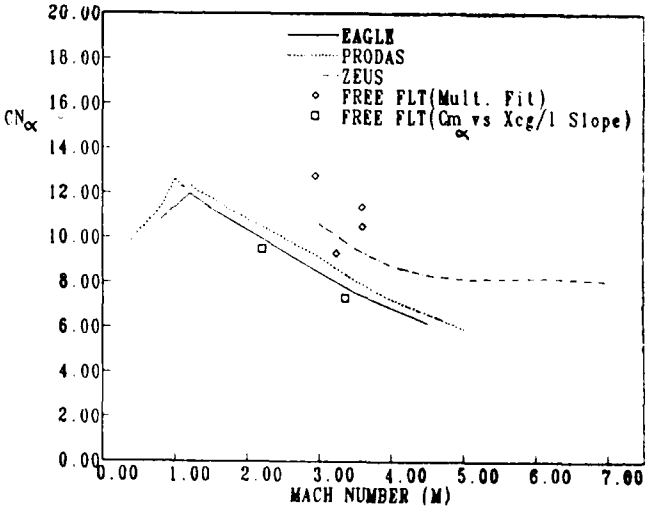

b. Large fin.

Fig. 8 Normal force derivatives.

The slope of the curve generated by the two center of gravity locations is a measure of the normal force coefficient derivative obtained from the following relationship:

$$C_{N_\alpha} = \frac{C_{m_\alpha}}{(l/d)(Xcg/l - Xcp/l)} \qquad (1)$$

where Xcp/l corresponds to where the curve crosses the X-axis at $C_{m_\alpha} = 0$. Using this approach and performing the calculation results in a C_{N_α} estimate of 9.06 for the small fin configuration at both M=1.2 and 2.2. The large fin configuration resulted in a C_{N_α} value of 9.45 at M=2.2 and a value of 7.29 at M=3.35. These values were confirmed further by inputing them in the analysis program, for each of the flights where the normal force was not experimentally accurately determined, and holding that value fixed. In each case, the probable error of fit (in swerve and angle) were not adversely affected and in most cases the fits benefited slightly. In addition, note that the multiple fit values shown in Figure 8 converged to solutions with C_{N_α} close to these. It is believed tha the scatter in the fitted values is caused by the relatively small angles of attack experienced during the flights resulting in very small lateral movement of the model. The lateral movement is the source of the fitted normal force derivatives. It shall be noted that blank values for C_{N_α} in the summary tables indicate that the empirically determined value was used and held constant during the fitting process. Because of the relatively large data scatter all that can be said for the comparison between the experimental data and the theoretical predictions are that the levels are in general agreement.

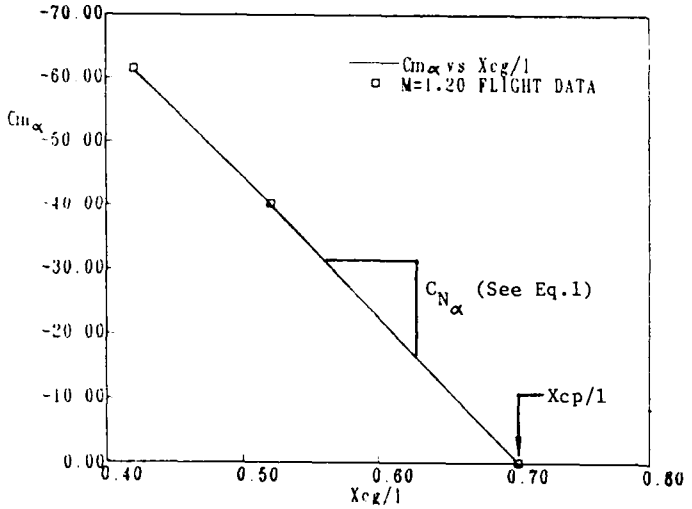

Fig. 9 Pitching moment versus Xcg slope yields normal force estimate.

Center of Pressure Location

Center of pressure location as a function of Mach number are presented in Figure 10 for the large and small fin configurations, respectively.

The experimental data shown in this figure was obtained from the previously discussed C_{m_α} and C_{N_α} results using the following relationships:

$$\frac{X_{cp}}{l} = \frac{-C_{m_\alpha}}{C_{N_\alpha}} \frac{d}{l} + \frac{X_{cg}}{l} \qquad (2)$$

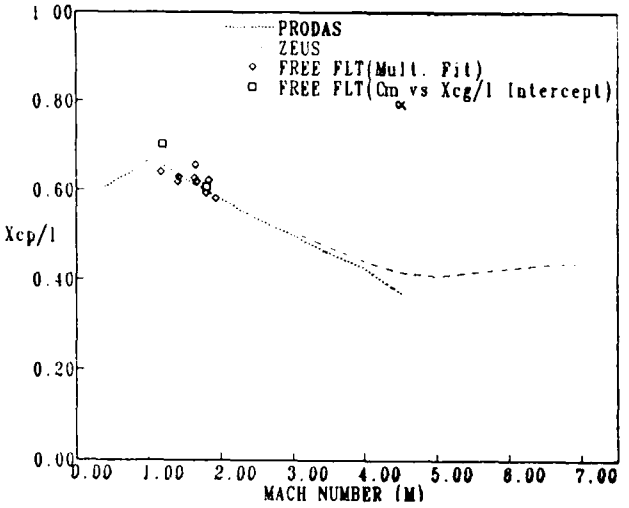

a. Small fin.

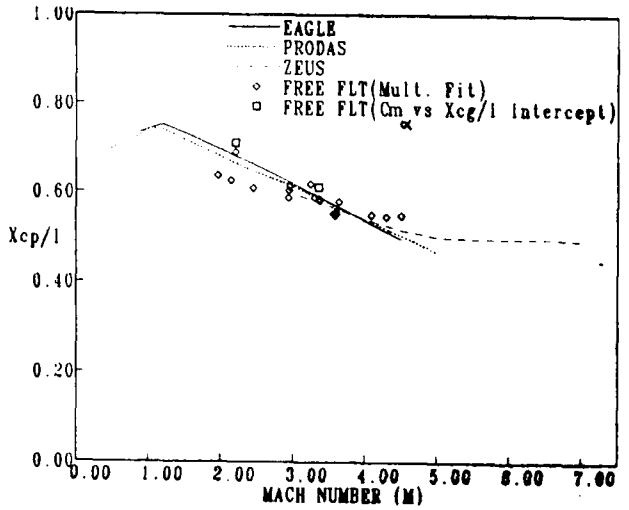

b. Large fin.

Fig. 10 Center of Pressure Location.

The PRODAS and EAGLE prediction for the large fin configuration compare well over the entire range of Mach numbers. ZEUS data converges with the EAGLE and PRODAS results in the region from M=3 to M=4.5, (see figure 10b). The same level of convergence for ZEUS and PRODAS is observed in figure 10a for the small fin model. The free-flight data for both fin configurations show good agreement between the theoretical and experimental results.

Axial Force Coefficient

The axial force coefficient (C_{xo}) is one of the easiest and most accurate coefficients to obtain from free flight aeroballistic tests. Figure 11 shows the experimentally obtained zero yaw axial force coefficients plotted versus Mach number. The EAGLE and PRODAS predictions are also plotted on this figure. The EAGLE prediction has been corrected by adding skin friction drag and base drag to the wave drag component computed by the inviscid EAGLE Flow solver.

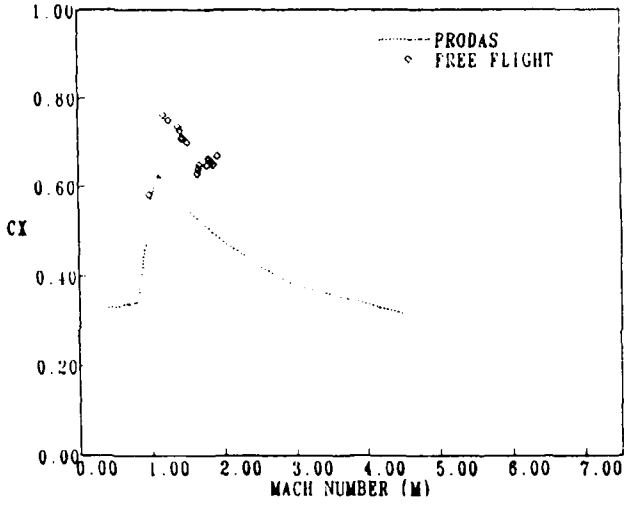

a. Small fin.

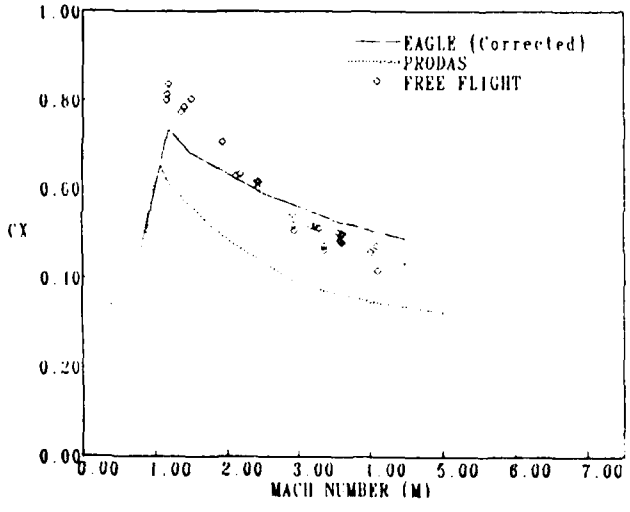

b. Large fin.

Fig. 11 Axial force coefficient.

The relationship chosen to model the turbulent skin friction coefficient has the following form:

$$CDf = \frac{0.455}{(\log R_l)^{2.58}} \left(\frac{S_w}{S_b}\right) \qquad (3)$$

Where S_w/S_b is the ratio of the wetted area to the base area of the model. Equation (3) is valid for Reynolds numbers ranging from 5×10^5 to 1×10^9. The flow over the entire surface of the model is assumed to be turbulent.[11]

The base drag component is obtained using one of two empirical relations depending on whether or not the flow is supersonic or subsonic:

$$\text{Subsonic, } C_{Db} = 0.029/\ C_{Df} \qquad (4)$$

$$\text{Supersonic, } C_{Db} = K\ (1.43/M^2) \qquad (5)$$

Where K is a function of Mach number.[11]

Figure 11b, which presents the results of the large fin analysis, shows good correlation of experimental free-flight data and corrected EAGLE results in the middle of the Mach number regime. Figure 12 presents the various components (C_{Df}, C_{Db}, and C_{Dw}) that make up the total theoretical drag coefficient and Figures 13 and 14 present the density contours for a typical transonic and supersonic EAGLE code analysis. Two different grid densities were used for these computations as previously discussed, and represents an attempt to tailor the grid to the desired flow field.

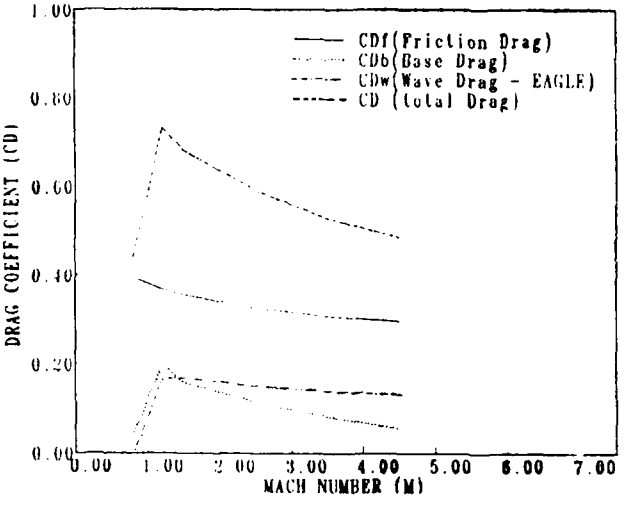

Fig. 12 Drag Components.

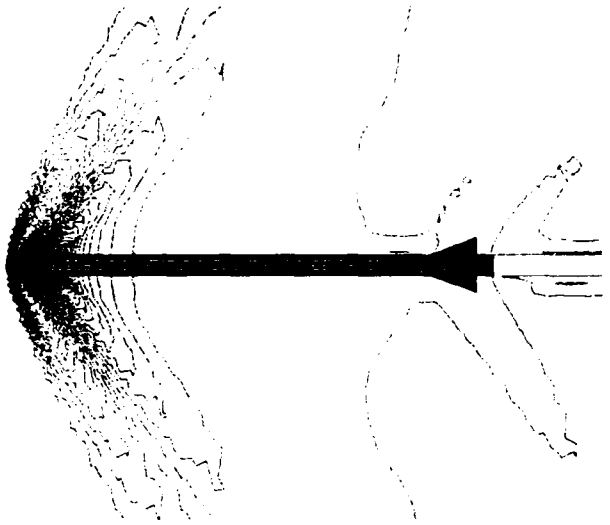

Fig. 13 Transonic Density Contour (α = 0.5 deg.)

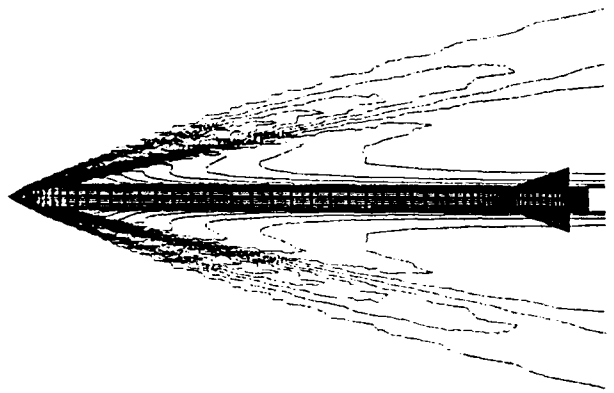

Fig. 14 Supersonic Density Contour (α = 0 deg.)

Roll Damping and Pitch Damping Derivative

The experimentally determined roll damping derivative (C_{lp}) and the pitch damping derivative (C_{mq}) are tabulated in Tables 1 and 2. Similarly, as for the other coefficients, a blank in the summary tables for these parameters means that they were held constant during the analysis of that flight. These results (both C_{lp} and C_{mq}) are not plotted herein because the ZEUS and EAGLE code predictions were not available. The ZEUS code is unable to accomplish these predictions and the predictions from the EAGLE code were not accomplished because these predictions require an unsteady, time dependant calculation which at present is not included in the routine.

Upon inspection of the C_{lp} data shown in Tables 1 and 2 these derivatives appear to have considerable scatter. This is believed to be caused by the very low roll rates experienced during the flights (i.e., the fins were not canted). It is significantly more difficult to extract C_{lp} from flights experiencing low roll rates because there is little rolling motion to be damped. This is analogous to determining the pitch damping derivative from flights with very low angular motion. The C_{mq} data tabulated in Tables 1 and 2 indicate that both the large and small fin models are dynamically stable. The vast majority of the experimentally obtained C_{mq} values lie between - 2000 and - 4000 per radian with no apparant effect due to fin size.

Conclusions

A comparison of experimental free-flight data with three different prediction routines have been accomplished for a slender fin stabilized missile configuration. These comparisons have been accomplished in the Mach number range of 1.0 to 5.0 and in general are in good agreement. All three prediction routines indicates that the static stability decreases rapidly with increasing Mach number and are consistant with the experimental data. Although the present analysis does not identify the cause of this decreasing static stability, it is apparantly not caused by flow viscous effects or the loss of fin effectiveness due to the boundary layer thickness. This is apparant because both the ZEUS and EAGLE codes are invisid routines and they predict this loss of static stability.

It is also of interest to note that the ZEUS code predicts that the forward shift of the center-of-pressure ceases near Mach five indicating that these high fineness ratio, tail control configurations may have applications in the hypersonic region. Unfortunately the present experimental data does not extend far enough into this region (above M=5) to confirm this trend. It is hoped that this will be accomplished in future tests. Also, the EAGLE code corrected for skin friction and base drag reasonably predicted the axial force coefficient. It is believed however, that this prediction could be further improved by using more sophisticated correction techniques. This is also an area were future work will be accomplished.

Although these tests were restricted to researching the stability characteristics of delta fin configurations, the test program is continuing to include other parameters. For example, the next phase (to be accomplished during the summer of 89) will investigate the potential advantage associated with moving more of the fin area outside the boundary layer. A clipped delta fin configuration has been fabricated which has the same fin area as the large delta fin models, while maintaining the fin span of the small delta fin models (described in this paper). In addition, an inverted fin model (where the root chord is very small compared to the tip chord) has been constructed which also has the same area and span constraints described above. It is hoped that the static stability of these configurations will be improved by moving more of the fin outside the boundary layer thus improving the model fin effectiveness. In addition to these near term tests, it is expected that testing will continue into future years where additional parameters will be investigated, such as fin longitudinal location, nose shape variations, and even flare variations.

Acknowledgments

Many individuals contributed to the various results presented in this paper. However, since all their names cannot be listed here, the authors would like to extend a special thanks to only a few. Mr Charlie Cottrell, AFATL/FXP, Eglin AFB. FL, produced the ZEUS predictions presented in this paper, Mr Wayne Hathaway, Arrow Tech, Burlington VT assisted in the reduction of the free-flight data, and finally Ms Cindi King, AFATL/FXA, Eglin AFB, FL for her patience in typing and preparing this paper.

Table 1 Experimental results (large fin)

M	$\bar{\delta}^2$	C_x	C_{N_α}	C_{m_α}	C_{mq}	C_{lp}	x_{cg}/l
SINGLE FITS							
1.175	0.0	0.800	---	---	---	---	0.83
1.180	0.0	0.813	---	---	---	---	0.83
1.200	0.0	0.836	---	---	---	-14.72	0.83
1.380	0.2	0.773	3.99	-92.91	-5843	---	0.83
1.424	0.5	0.784	---	---	---	-12.02	0.83
1.519	0.7	0.803	---	-98.84	-4741	-14.31	0.83
1.950	0.9	0.705	16.89	-81.52	---	-12.72	0.83
2.137	4.5	0.628	17.28	-83.60	---	---	0.52
2.220	1.4	0.633	10.42	-64.92	-3837	---	0.83
2.424	0.3	0.616	5.36	---	---	---	0.83
2.441	2.3	0.602	18.95	-63.75	-2833	---	0.83
2.458	0.5	0.614	19.19	-59.03	-2816	---	0.83
2.931	4.6	0.543	16.48	-26.36	---	-11.71	0.52
2.944	8.7	0.505	10.77	-23.76	-3351	-11.07	0.52
3.184	30.4	0.516	---	-43.13	---	---	0.83
3.292	1.3	0.510	10.36	-39.49	-3154	-7.38	0.83
3.355	3.8	0.463	10.17	-15.59	-2817	-10.00	0.52
3.359	1.0	0.470	11.74	-42.47	-1802	---	0.83
3.361	28.6	0.502	10.53	-30.65	-2307	-12.32	0.83
3.573	3.2	0.484	12.05	-34.33	-2108	---	0.83
3.616	4.8	0.479	---	-32.91	-2876	-5.85	0.83
3.629	11.2	0.499	8.70	-30.95	---	---	0.83
4.005	3.9	0.458	1.87	-23.58	-3882	---	0.83
4.086	29.1	0.472	8.93	-15.16	---	-2.19	0.52
4.089	3.2	0.416	8.38	-24.12	---	-3.72	0.83
4.503	8.3	0.430	8.12	-23.02	-2997	-5.91	0.83
MULTIPLE FITS							
2.937	7.6	0.516	12.74	-25.37	-2491	-11.22	0.52
3.237	17.9	0.518	9.29	-41.93	---	-7.06	0.83
3.588	17.9	0.482	11.37	-32.80	-2458	-6.32	0.83
3.595	19.4	0.498	10.47	-31.17	-2038	-10.79	0.83

Table 2 Experimental results (small fins)

M	$\bar{\delta}^2$	C_x	C_{N_α}	C_{m_α}	C_{mq}	C_{lp}	x_{cg}/l
SINGLE FITS							
0.966	1.0	0.581	----	-49.25	----	----	0.52
1.177	1.0	0.761	8.58	-43.22	-1484	-6.87	0.52
1.288	0.2	0.749	----	-68.72	----	-3.82	0.83
1.383	0.9	0.734	----	-57.82	----	----	0.83
1.427	4.3	0.707	10.65	-50.89	-2733	-8.85	0.83
1.442	21.3	0.709	----	-33.37	----	----	0.52
1.504	29.9	0.699	----	-25.90	-2625	----	0.52
1.638	2.8	0.628	9.60	-28.53	-2832	-2.82	0.52
1.673	2.3	0.648	5.80	-28.52	-2846	-5.26	0.52
1.778	7.0	0.647	----	-21.06	- 981	----	0.52
1.794	19.0	0.662	8.22	-14.37	-2429	-4.54	0.52
1.814	0.7	0.660	----	-39.99	----	-9.55	0.83
1.868	1.6	0.648	6.31	-42.68	-3182	-5.93	0.83
1.928	8.9	0.668	11.28	-40.86	-1860	-3.09	0.83
MULTIPLE FITS							
1.404	2.6	0.725	11.77	-53.48	-2694	-4.54	0.83
1.656	2.4	0.639	7.30	-23.86	-2547	-2.89	0.52
1.840	1.1	0.655	9.15	-42.22	-2822	-6.41	0.83

References

1. Swift, H. F., McDonald, J. W., Chelekis, R. M., "Description and Capabilities of a Two-Stage Light Gas Launcher," Presented at the 35th Aeroballistic Range Association Meeting, Meppen, Federal Republic of Germany, September 1984.

2. Kittyle, R. L., Packard, J. D., Winchenbach, G. L., "Description and Capabilities of the Aeroballistic Research Facility," AFATL-TR-87-08, May 1987.

3. Fischer, M. A., Hathaway, W. H., "Aeroballistic Research Facility Data Analysis System (ARFDAS)," AFATL-TR-88-48, September 1988.

4. Hathaway, W. H., Whyte, R. H., Burnett, J. R., "Projectile Design Analysis System (PRODAS)," Presented at the 31st Aeroballistic Range Association Meeting, Pasadena, California, October 1980.

5. Wardlaw, A. B., Davis, S. F., Priolo, F. J., "A Second Order Gudunov's Method for Supersonic Tactical Missile Computations," Naval Surface Warfare Center, TR 86-506, December 1986.

6. Wardlaw, A. B., Priolo, F. J., "Applying the ZEUS Code," Naval Surface Warfare Center, TR 86-508, December 1986.

7. Lijewski, L., Cipolla, J. et al., "Program EAGLE User's Manaul, Volume I - Introduction and Grid Applications", AFATL-TR-88-117, Volume I, September 1988.

8. Thompson, J. F., and Gatlin, B., "Program EAGLE User's Manual, Volum II - Surface Generation Code", AFATL-TR-88-117, Volume II, September 1988.

9. Thompson, J. F., and Gatlin, B., "Program EAGLE User's Manual, Volume III - Grid Generation Code", AFATL-TR-88-117, Volume III, September 1988.

10. Mounts, J. S., Belk, D. M., and Whitfield D. L., "Program EAGLE User's Manual, Volume IV - Multiblock Implicit, Steady State Euler Code", AFATL-TR-88-117, Volume IV, September 1988.

11. Hoerner, Sighard, "Fluid Dynamic Drag", Hoerner Fluid Dynamics, 1965.